

Metal adatoms on graphene and hexagonal boron nitride: Towards the rational design of self-assembly templates

Oleg V. Yazyev* and Alfredo Pasquarello

*Institute of Theoretical Physics, Ecole Polytechnique Fédérale de Lausanne (EPFL), CH-1015 Lausanne, Switzerland and
Institut Romand de Recherche Numérique en Physique des Matériaux (IRRMA), CH-1015 Lausanne, Switzerland*

(Dated: October 31, 2018)

Periodically corrugated epitaxial graphene and hexagonal boron nitride (*h*-BN) on metallic substrates are considered as perspective templates for the self-assembly of nanoparticles arrays. By using first-principles calculations, we determine binding energies and diffusion activation barriers of metal adatoms on graphene and *h*-BN. The observed chemical trends can be understood in terms of the interplay between charge transfer and covalent bonding involving the adatom *d* electrons. We further investigate the electronic effects of the metallic substrate and find that periodically corrugated templates based on graphene in combination with strong interactions at the metal/graphene interface are the most suitable for the self-assembly of highly regular nanoparticle arrays.

PACS numbers: 36.40.Sx, 61.48.De, 68.43.Bc, 68.65.Cd

I. INTRODUCTION

Two-dimensional graphene and hexagonal boron nitride (*h*-BN) are attracting considerable attention due to their extraordinary physical properties and perspective technological applications.^{1,2} Epitaxial single layers of graphene and *h*-BN can be grown via the chemical vapor deposition route on a large variety of metallic substrates.³ In many cases, the epitaxial layers of these two materials are extremely well-ordered but reveal long-wavelength periodic corrugations, or Moiré patterns, resulting from the lattice constant mismatch.^{4–7} Such superlattices are considered as promising templates for the chemical self-assembly of periodic arrays of nanoparticles, with perspective applications in ultra-high density information storage, catalysis, sensing, etc.⁸ The potential of this approach has already been affirmed by the successful production of regular arrays of nanoclusters with narrow size distributions.^{9–12}

One attractive property of this approach to nanoscale self-assembly is the high degree of customization. Indeed, the space of allowed chemical compositions involves three degrees of freedom: (*i*) deposited metallic nanoparticles formed by virtually any metal from the periodic table; (*ii*) a monolayer of either graphene or *h*-BN; (*iii*) metallic surfaces, one of the many (111) fcc or (0001) hcp surfaces of forth or fifth row late transition metals. Understanding the roles these three factors play in the self-assembly process is of paramount importance for the rational design of nanoparticle arrays with novel properties and functions.

In this work, we aim at understanding the chemical trends in the binding and diffusion of individual metal adatoms, the initial step which largely predetermines the overall self-assembly process. In particular, by using first-principles calculations we perform a systematic study of the adatom binding and diffusion as well as of the electronic properties of the metal adatoms upon deposition. First, we focus on the chemical trends observed for metal adatoms varying horizontally and vertically in the periodic table, when absorbed on free-standing graphene and

h-BN. Then, we model the electronic effects of periodically corrugated epitaxial layers deposited on two metallic substrates representing the limiting cases of strong and weak interactions at the interface.

The present paper is organized as follows. In Sec. II we describe our first-principles methodology and the adopted models. Section III discusses the binding and the diffusion of adatoms on free-standing graphene and *h*-BN. Section IV is devoted to the investigation of substrate effects. The conclusions are drawn in Sec. V.

II. METHODS

In our approach, the electronic structure is described through the use of the Perdew-Burke-Ernzerhof (PBE) exchange-correlation density functional within density functional theory.¹³ The ultrasoft pseudopotentials¹⁴ used in the present study treat the *d*-electrons of all transition metals as valence electrons. The semi-core *sp*-states were also treated explicitly in the case of early third row elements (K–Fe). The one-electron valence wave functions and the electron density were described by plane-wave basis sets with kinetic energy cutoffs of 30 Ry and 300 Ry, respectively.¹⁵ All calculations were performed using the spin-unrestricted formalism. We used the PWSCF plane-wave pseudopotential code of the QUANTUM-ESPRESSO distribution.¹⁶ The convergence of the results with respect to the simulation parameters was systematically verified.

The constructed models are based on periodic two-dimensional 3×3 supercells in combination with 4×4 **k**-point meshes. Potential energy surfaces for the free-standing graphene and *h*-BN systems were studied by relaxing all atomic positions with the initial coordinates of the adatom set to the high-symmetry positions shown in Fig. 1. This procedure allowed us to determine both the potential energy surface minima and the transition state configurations connecting the neighboring equivalent minima, since symmetry was retained during the

relaxation. The validity of this approach was verified through nudged elastic band calculations.¹⁷ For specific cases, we could compare our results with those of other investigations,^{18,19} finding good agreement.

We investigated the effects of local electronic-structure variations due to the presence of metallic substrates by considering the case of Co adatoms on epitaxial graphene and *h*-BN supported by lattice-matched Ni(111) and Cu(111) substrates. These metallic substrates correspond to regimes of strong and weak monolayer-substrate interactions, respectively.²⁰ Under realistic conditions these metals do not produce Moiré pattern due to the small lattice mismatch.^{3,21–23} However, through models involving such structures, we could study electronic effects induced by the Moiré superlattice using sufficiently small simulation cells and without introducing large lateral strains. A very similar methodology was also used in Ref. 4. The considered model calculations consist of 3×3 two-dimensional slabs composed of 4 atomic planes of metal with both surfaces covered by graphene or *h*-BN in order to avoid spurious dipole-dipole interactions. The slab configurations were fully optimized, including the distance between the metal layers.²⁴

III. ADATOMS ON SUSPENDED GRAPHENE AND *h*-BN

First, let us compare the potential energy surfaces (PES) for a representative case of a Co adatom on freestanding graphene and *h*-BN (Fig. 1). For both monolayers the PES minima correspond to the hollow (*h*) sites. Interestingly, in the case of Co as well as for most of the other metal adatoms the distortions of the graphene and *h*-BN lattices are very weak. Although the two PES involving the Co adatom are qualitatively similar, the binding energy on graphene are substantially higher (1.60 eV vs. 1.03 eV). The stronger binding to graphene is a systematic feature which can be understood considering that the chemisorption of metal adatoms is governed by the following attractive contributions: (i) strong covalent bonding, and (ii) moderate electrostatic interaction as a result of charge transfer between the adatom and the monolayer. While graphene is a semimetal, *h*-BN is an insulator with a band gap of ≈ 6 eV.²⁵ The availability of low-energy electronic states in graphene results in a more efficient interaction with the adatom states and allows for charge transfer between the graphene layer and the adatom, thus introducing an electrostatic component. The preferential binding to the *h* sites is very common, although we find a number of exceptions, especially among the heavy transition metals. In particular, for Pd, Ir and Pt, the bridge (*b*) site is the lowest energy position on graphene. The nitrogen on-top sites (t_N) correspond to the PES minima on *h*-BN for V, Ni, Pd, Ir and Pt.

The lowest energy pathways connecting the neighboring local minima involve transition states at *b* and t_B sites for the Co adatom on graphene and *h*-BN, respec-

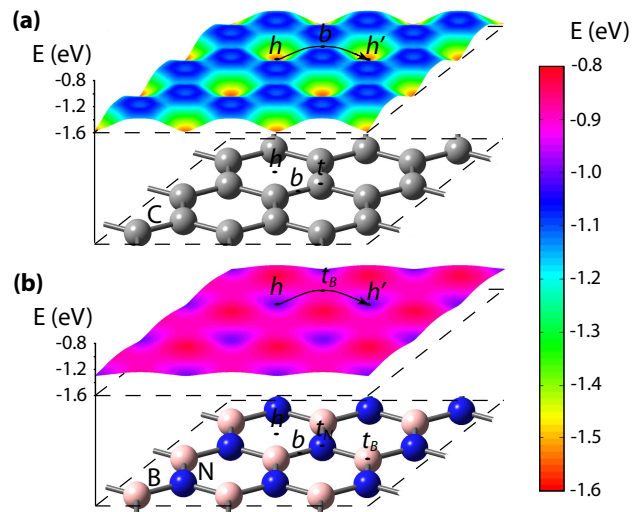


FIG. 1: (Color online) Potential energy surfaces of the Co adatom on freestanding (a) graphene and (b) *h*-BN obtained by constraining the in-plane position of the Co adatom on a 6×6 points mesh in the unit cell. The same energy scale is used in both plots and the energy is referred with respect to that of an isolated Co atom. The high-symmetry positions are indicated with labels. The arrows show the lowest energy diffusion pathways connecting the local minima, *h* sites, through the transition state configurations, the *b* sites and t_B sites in the case of graphene and *h*-BN, respectively.

tively. The diffusion activation barriers are again higher for graphene, 0.40 eV vs. 0.13 eV for *h*-BN. However, this trend is not systematic across the periodic table and very often the diffusion on *h*-BN is characterized by higher activation barriers [cf. Fig. 2(a,b)]. Notably, the calculated activation barrier in the case of *h*-BN agrees well with the experimental value of 0.14 ± 0.03 eV for the diffusion of Co adatoms on *h*-BN deposited on Ni(111).²⁶

Figure 2(a) shows the horizontal trend in the binding energies and the diffusion activation barriers across the third row of the periodic table. Both graphene and *h*-BN show double-peaked features with maximum binding energies at Ti and Ni which have d^2 and d^8 electronic configurations, respectively, while the very weak binding of Cr and Mn corresponds to the situation of half-filled *d*-shells. Strong binding energies with magnitudes up to 2.08 eV (1.14 eV) for graphene (*h*-BN) indicate the contribution from covalent binding involving *d* electrons. However, the fact that the atomic magnetic moments due to the partially filled *d*-shells are largely preserved upon binding [Fig. 2(c)] shows that graphene and *h*-BN act as weak ligand fields with respect to the metal adatoms. Large magnetic moments associated to half-filled *d*-shell elements correspond to large values of spin splitting of *d*-electron states and, thus, to their reduced participation to the covalent binding. The other elements in the first (second) half of the transition metal series tend to give enhanced (reduced) magnetic moments upon binding. To elucidate the origin of this behavior, we per-

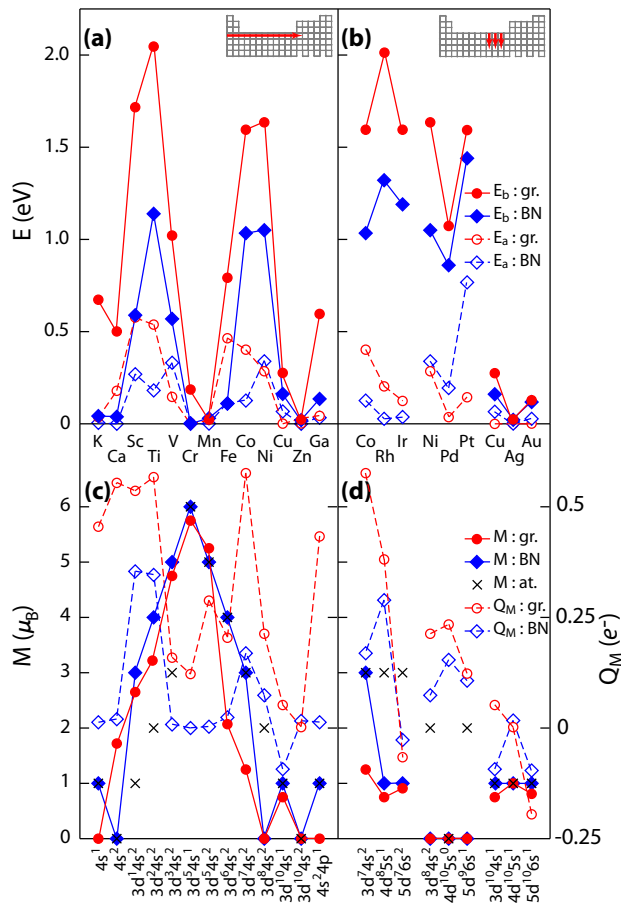


FIG. 2: (Color online) (a) Horizontal and (b) vertical chemical trends in the binding energies E_b and the diffusion activation barriers E_a of metal adatoms on graphene and *h*-BN. Insets show the concerned parts of the periodic table: K–Ga in (a) and Co–Ir, Ni–Pt, Cu–Au in (b). (c) Horizontal and (d) vertical chemical trends in the magnetic moments M and the atomic charges Q_M of the adsorbed metal adatoms in their lowest energy configurations. Crosses refer to the magnetic moments of isolated atoms. Electronic configurations of the isolated atoms are given at the bottom of the figure for reference.

formed the Löwdin population analysis²⁷ and found that the adsorption of metal adatoms leads to the partial promotion of electrons from the *s*- to the *d*-shell thus leading to the observed changes of the magnetic moments.

Such trends depending on the partial *d*-shell filling appear to be generic since a very similar behavior was found for metal-benzene molecular complexes²⁸ and even for strongly bound substitutional impurities in graphene.^{29–31} The binding energies on *h*-BN as well as the activation barriers on both monolayers follow exactly the same qualitative trend within the transition metal series (Sc–Zn). Outside of this region (K, Ca and Ga) only graphene is able to bind adatoms strongly since the interactions are then governed by the sole electrostatic contribution resulting from charge transfer. This contrast is well illustrated by comparing the Löwdin atomic charges

Q_M of metal adatoms on the two monolayers [Fig. 2(c)].

Vertical trends in the periodic table are illustrated in Fig. 1(b) for the late transition and coinage metal adatoms. In general, the binding energies tend to increase when moving down the columns of the periodic table. The reductions can be associated with the changes of the lowest energy adsorption sites discussed above. The largest binding energy of 2.02 eV is found for Rh on graphene while the highest activation barrier of 0.77 eV corresponds to Pt on *h*-BN. At variance, the diffusion of Pd on graphene and of Rh and Ir on *h*-BN are characterized by very low diffusion barriers (<0.05 eV) combined with high binding energies (>1 eV). Inert coinage metals have very low binding energies and diffusion barrier, with minimum values for Ag. Similar trends were also observed for carbon on coinage metal surfaces.³² Even on graphene, Ag shows practically no charge transfer as this element is located at the point of crossover between electron donating (Cu) and electron accepting (Au) behavior [Fig. 2(d)]. The hole-doping of graphene which is otherwise difficult to achieve by chemical means was recently demonstrated in Au deposition experiments.³³ Interestingly, we find that also strongly binding Ir adatoms act as electron acceptors.

It is worth stressing that the presently used theory does not provide a correct description of weak van der Waals interactions. This might quantitatively affect the results, especially when the considered adatom does not give rise to strong covalent bonding and/or electrostatic interactions.

IV. EFFECT OF METALLIC SUBSTRATE

On the surfaces of forth and fifth row transition metals, epitaxial graphene and *h*-BN produce Moiré patterns due to the mismatch between the lattice constants of the substrate and of the monolayer [cf. Fig. 3(a)]. The local shifts of the monolayer lattice with respect to the substrate lattice across the Moiré unit cell result in long-wavelength modulations of the PES which drive the self-assembly of periodic arrays of nanoparticles. These modulations are due to variations in the monolayer-substrate distance and to changes in the local electronic structure.⁶ Below, we focus on the role of local electronic structure variations in the diffusion of individual metal adatoms on metal-supported graphene and *h*-BN. Collective effects due to the local rehybridization induced by few-atom clusters have been considered elsewhere.^{34,35} In addition, the distance modulations alone can lead to only minor curvature-induced effect on the adatom binding energies since the estimated height variations are actually rather small ($\Delta h < 1.5$ Å^{4,7}) compared to the size of the Moiré unit cell ($a \sim 3$ nm).³⁶

In order to understand the effect of the local electronic structure variations, we study the binding of Co adatoms on epitaxial graphene and *h*-BN supported by lattice-matched Ni(111) and Cu(111) substrates. These two

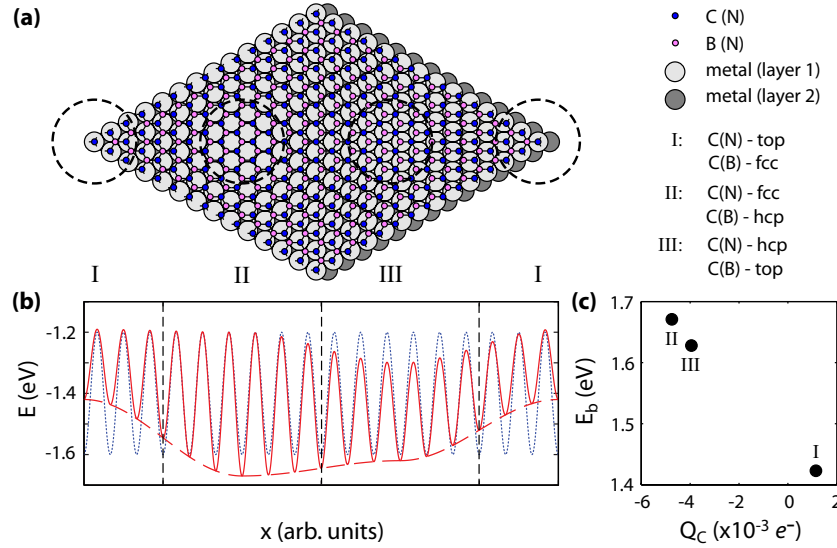


FIG. 3: (Color online) (a) Schematic illustration of the Moiré unit cell with three binding regions indicated. (b) Schematic representation of the potential energy surface (solid line) for the diffusion of the adatom moving along the horizontal direction of the unit cell shown in (a), based on calculations for Moiré domains I–III. The actual local binding energies (dashed line) and diffusion barriers (oscillation amplitudes) correspond to the case of the Co adatom on graphene supported by Ni(111). The dotted line refers to the case of the Co adatom on free-standing graphene. (c) Binding energy E_b of the Co adatom versus the charge transfer per carbon atom Q_C from the metal to graphene for the three Moiré domains.

cases model the regimes of strong and weak monolayer-substrate interactions, respectively.²⁰ We stress that under realistic conditions these metals do not produce Moiré pattern due to the small lattice mismatch.^{3,21–23} The three principal Moiré domains [I–III in Fig. 3(a)] are modeled by introducing an artificial lateral shift between the monolayer and the substrate. Further details of this procedure are given in Sec. II.

The calculated binding energies and activation barriers for Co adatoms on graphene|Ni(111) show appreciable variation across the three Moiré domains [cf. Table I]. The resulting PES [schematically depicted in Fig. 3(b)] can be viewed as a modulation of the PES of free-standing graphene [Fig. 1(a)] by the long-wavelength perturbations resulting from the periodicity of the Moiré superlattice. The Moiré domain I, which is characterized by the shortest graphene-substrate distance (2.23 Å),^{37–39} shows the lowest binding energy while the opposite is true for region II showing the largest graphene-substrate distance (4.11 Å). However, Moiré domain III presents a short graphene-substrate distance (2.49 Å) in combination with a high binding energy [Table I], indicating that there is no clear correlation between these quantities. At variance, a clear correlation can be established between the binding energies of the Co adatoms and the local charge transfer per carbon atom (Q_C) from the metal to graphene [cf. Fig. 3(c)]. This result can be intuitively understood: the charge transfer from the metal to graphene reduces the charge transfer from the Co adatom to the template surface and, thus, the electrostatic component of the binding energy. Very recently a similar electrostatic effect has also been found for adatoms on ultra-

thin oxide films.⁴⁰ For Co adatoms on *h*-BN|Ni(111), we found the same tendency, although the local variations of the binding energy are smaller in this case. On a weakly binding substrate such as the Cu(111) surface, the PES remains practically unchanged across the Moiré unit cell.

The Moiré domains associated with higher binding energies are expected to show larger thermal populations of adatoms, and will thus act as nucleation centers for nanoparticles. Therefore, larger variations of the binding energies across the Moiré template will favor more ordered nanoparticle arrays with narrower size distributions. We conclude that the templates made of graphene in combination with strongly binding metal surfaces (e.g. Ir, Rh, Ru) are more promising for the self-assembly of metal nanoparticle arrays.

TABLE I: Comparison of binding energies E_b (in eV) and diffusion activation barriers E_a (in eV) of the Co adatom on free-standing graphene (gr.) and *h*-BN with corresponding epitaxial monolayers deposited on Ni(111) and Cu(111). The different positions of the monolayer atoms refer to three distinct local regions of the Moiré pattern shown in Fig. 3.

Moiré domain	E_b			E_a		
	I	II	III	I	II	III
gr.		1.60			0.40	
gr. Ni(111)	1.42	1.67	1.62	0.23	0.47	0.32
gr. Cu(111)	1.66	1.67	1.67	0.45	0.45	0.45
<i>h</i> -BN		1.03			0.13	
<i>h</i> -BN Ni(111)	0.86	0.89	0.88	0.10	0.14	0.14
<i>h</i> -BN Cu(111)	1.17	1.17	1.17	0.16	0.20	0.20

V. CONCLUSIONS

We systematically studied the potential energy surfaces of metal adatoms on graphene and *h*-BN across the periodic table, and clarified the role of the metallic substrate in adatom diffusion. The present results are well understood within a simple picture involving covalent and electrostatic interactions. Our work formulates general principles required for the rational design of self-assembly templates based on epitaxial graphene and *h*-

BN which can find applications in ultra-high density information storage, catalysis and sensing, and so on.

ACKNOWLEDGMENTS

We acknowledge fruitful discussions with H. Brune, P. Bulushek, R. Decker, A. Lehnert, and S. Rusponi. The calculations were performed at the CSCS.

-
- * Present address: Department of Physics, University of California, Berkeley, CA 94720, USA; E-mail: yazyev@civet.berkeley.edu
- ¹ A. K. Geim and K. S. Novoselov, *Nature Mater.* **6**, 183 (2007).
 - ² M. I. Katsnelson, *Materials Today* **10**, 20 (2007).
 - ³ C. Oshima and A. Nagashima, *J. Phys.: Condens. Matter* **9**, 1 (1997).
 - ⁴ R. Laskowski, P. Blaha, T. Gallauner, and K. Schwarz, *Phys. Rev. Lett.* **98**, 106802 (2007).
 - ⁵ J. Coraux, A. T. N'Diaye, C. Busse, and T. Michely, *Nano Lett.* **8**, 565 (2008).
 - ⁶ A. L. Vázquez de Parga, F. Calleja, B. Borca, M. C. G. Passeggi, J. J. Hinarejos, F. Guinea, and R. Miranda, *Phys. Rev. Lett.* **100**, 056807 (2008).
 - ⁷ D. Martocchia, P. R. Willmott, T. Brugger, M. Björck, S. Gunther, C. M. Schlepütz, A. Cervellino, S. A. Pauli, B. D. Patterson, S. Marchini, J. Wintterlin, W. Moritz, and T. Greber, *Phys. Rev. Lett.* **101**, 126102 (2008).
 - ⁸ S. Berner, M. Corso, R. Widmer, O. Groening, R. Laskowski, P. Blaha, K. Schwarz, A. Goriachko, H. Over, S. Gsell, M. Schreck, H. Sachdev, T. Greber, and J. Osterwalder, *Angew. Chem. Int. Ed.* **46**, 5115 (2007).
 - ⁹ A. T. N'Diaye, S. Bleikamp, P. J. Feibelman, and T. Michely, *Phys. Rev. Lett.* **97**, 215501 (2006).
 - ¹⁰ J. Zhang, V. Sessi, C. H. Michaelis, I. Brihuega, J. Honolka, K. Kern, R. Skomski, X. Chen, G. Rojas, and A. Enders, *Phys. Rev. B* **78**, 165430 (2008).
 - ¹¹ A. T. N'Diaye, T. Gerber, C. Busse, J. Mysliveček, J. Coraux, and T. Michely, *New J. Phys.* **11**, 103045 (2009).
 - ¹² K. Donner and P. Jakob, *J. Chem. Phys.* **131**, 164701 (2009).
 - ¹³ J. P. Perdew, K. Burke, and M. Ernzerhof, *Phys. Rev. Lett.* **77**, 3865 (1996).
 - ¹⁴ D. Vanderbilt, *Phys. Rev. B* **41**, 7892 (1990).
 - ¹⁵ A. Pasquarello, K. Laasonen, R. Car, C. Lee, and D. Vanderbilt, *Phys. Rev. Lett.* **69**, 1982 (1992); K. Laasonen, A. Pasquarello, R. Car, C. Lee, and D. Vanderbilt, *Phys. Rev. B* **47**, 10142 (1993).
 - ¹⁶ P. Giannozzi *et al.*, *J. Phys.: Condens. Matter* **21**, 395502 (2009); <http://www.quantum-espresso.org/>.
 - ¹⁷ G. Mills, H. Jónsson, and G. K. Schenter, *Surf. Sci.* **324**, 305 (1995).
 - ¹⁸ K. T. Chan, J. B. Neaton, and M. L. Cohen, *Phys. Rev. B* **77**, 235430 (2008).
 - ¹⁹ H. Sevinçli, M. Topsakal, E. Durgun, and S. Ciraci, *Phys. Rev. B* **77**, 195434 (2008).
 - ²⁰ G. Giovannetti, P. A. Khomyakov, G. Brocks, V. M. Karpan, J. van den Brink, and P. J. Kelly, *Phys. Rev. Lett.* **101**, 026803 (2008).
 - ²¹ A. Nagashima, N. Tejima, and C. Oshima, *Phys. Rev. B* **50**, 17487 (1994).
 - ²² Y. Gamo, A. Nagashima, M. Wakabayashi, M. Terai, and C. Oshima, *Surf. Sci.* **374**, 61 (1997).
 - ²³ X. Li, W. Cai, J. An, S. Kim, J. Nah, D. Yang, R. Piner, A. Velamakanni, I. Jung, E. Tutuc, S. K. Banerjee, L. Colombo, and R. S. Ruoff, *Science* **324**, 1312 (2009).
 - ²⁴ K. Kádas, Z. Nabi, S.K. Kwon, L. Vitos, R. Ahuja, B. Johansson, and J. Kollár, *Surf. Sci.* **600**, 395 (2006).
 - ²⁵ B. Arnaud, S. Lebegue, P. Rabiller, and M. Alouani, *Phys. Rev. Lett.* **96**, 026402 (2006).
 - ²⁶ W. Auwärter, M. Muntwiler, T. Greber, and J. Osterwalder, *Surf. Sci.* **511**, 379 (2002).
 - ²⁷ P.-O. Löwdin, *J. Chem. Phys.* **18**, 365 (1950).
 - ²⁸ R. Pandey, B. K. Rao, P. Jena, and M. A. Blanco, *J. Am. Chem. Soc.* **123**, 3799 (2001).
 - ²⁹ A. V. Krasheninnikov, P. O. Lehtinen, A. S. Foster, P. Pyykko, and R. M. Nieminen, *Phys. Rev. Lett.* **102**, 126807 (2009).
 - ³⁰ E. J. G. Santos, A. Ayuela, and D. Sánchez-Portal, *New J. Phys.* **12**, 053012 (2010).
 - ³¹ D. W. Boukhvalov and M. I. Katsnelson, *Appl. Phys. Lett.* **95**, 023109 (2009).
 - ³² O. V. Yazyev and A. Pasquarello, *Phys. Rev. Lett.* **100**, 156102 (2008).
 - ³³ I. Gierz, C. Riedl, U. Starke, C. R. Ast, and K. Kern, *Nano Lett.* **8**, 4603 (2008).
 - ³⁴ P. J. Feibelman, *Phys. Rev. B* **77**, 165419 (2008).
 - ³⁵ P. J. Feibelman, *Phys. Rev. B* **80**, 085412 (2009).
 - ³⁶ We assume spherically curved regions of diameter $d=a/2$. The estimated curvature radius $R \approx a^2/(32\Delta h) \geq 2$ nm is too large to produce any sizable effect on the local binding energies.⁴¹
 - ³⁷ G. Bertonni, L. Calmels, A. Altibelli, and V. Serin, *Phys. Rev. B* **71**, 075402 (2005).
 - ³⁸ V. M. Karpan, G. Giovannetti, P. A. Khomyakov, M. Talanana, A. A. Starikov, M. Zwierzycki, J. van den Brink, G. Brocks, and P. J. Kelly, *Phys. Rev. Lett.* **99**, 176602 (2007).
 - ³⁹ O. V. Yazyev and A. Pasquarello, *Phys. Rev. B* **80**, 035408 (2009).
 - ⁴⁰ L. Giordano, G. Pacchioni, J. Goniakowski, N. Nilius, E. D. L. Rienks, and H.-J. Freund, *Phys. Rev. Lett.* **101**, 026102 (2008).
 - ⁴¹ F. J. Ribeiro, J. B. Neaton, S. G. Louie, and M. L. Cohen, *Phys. Rev. B* **72**, 075302 (2005).